Electronic Supplementary Material (ESI) for ChemComm.

Supporting Information

Combined antioxidant capped and surface supported redox-sensitive nanoparticles for continuous elimination of multi-metallic species

Section S1: Materials and methods

Materials and chemicals

Shells intact Tulsi Sitarbai almonds were obtained from a local shop. Chemicals purchased were atleast of analytical purity. Quartz sand (50-70 mesh) was obtained from Sigma Aldrich (US). Other chemicals were procured from Merck and include- methanol, ethanol, $FeCl_3.6H_2O$, $NaBH_4$, HCl, NaOH, $K_2Cr_2O_7$, $NaAsO_2$ solution, $Ni(NO_3)_2.6H_2O$, and $CdCl_2.H_2O$.

Pre-processing, and materials synthesis

Low temperature pyrolysis of crushed almond shells i.e. at 550^0C for 3h, resulted in formation of multifunctional biochar surface. It was washed using 1M HCl to remove the impurities followed by multiple washes with deionized water. Hot water blanching method was used to peel of and separate the almond skins. They were dried in sunlight and crushed before antioxidants extraction. 2 gm of almond skin powder was reacted with a total of 80 mL (in four cycles) of 1000:1 methanol: HCl mixture using continuous sonication [1].

Biochar powder was interacted with the antioxidant extract to generate the final surface utilized in supporting the Fe^0 NPs. Fe/BC mass ratio=1 was taken in a 4:1 ethanol: water solution was taken and continuous sonication and shaking (30 min each) was provided to assure the interaction of iron ions with the surface.

After that, 0.94M $NaBH_4$ solution was reacted dropwise to start the reduction reaction. After complete addition, the reaction mixture was further stirred for another 20 minutes to assure complete reduction of iron. Reaction precipitate was filtered and washed with ethanol and water [2]. Obtained mixture was immediately added to the antioxidant extract solution to cap the grown Fe^0 particles.

Finally, the precipitate was filtered, washed and vacuum dried before further use.

Materials characterization

Synthesized composites and raw materials were characterized for morphology and composition using scanning (Carl Zeiss SUPRA 55VP FESEM) and transmission electron microscopy (UHR-FEG-TEM, JEOL, JEM 2100 F model using a 200 kV electron source) both associated with EDAX (Oxford INCA).

Materials crystallinity and phase information was obtained using powder x-ray diffraction analysis with Rigaku (mini flex, Japan) benchtop powder X-ray diffractometer having Cu Kα = 1.54059 Å radiation at 40 kV/15 mA. Data collection was done in range of 5^o to 65^o 2θ at a scanning rate of 5° 2θ per minute. Information about the surface functional groups was obtained using Fourier transformation infrared spectroscopy (FTIR). For almond skins before and after the extraction of antioxidants ATR mode was used whereas in biochar and composite characterization KBr pellet method was utilized. Almond skin extracts (Antioxidants) concentrations were qualitatively observed using UV-Vis spectrophotometer (Evolution 201, Thermoscientifc) before and after the modification of nanocomposite. Zeta potential analysis was performed using Malvern ZetaSizer ZS-90 (Malvern).

Batch and column sorption tests

For kinetic experiments, 20 mg of SA-Fe^0 was reacted with 20 mL of 0.01M $NaNO_3$ solution (pH= 6.5) containing 20 mg/L of each of the four metal species for varying time (2 min- 360 min) at 25^0C and 200 RPM. Kinetics data was modelled using General order kinetic model to obtain the rate constant and the order of the reaction.

Logically the order of a chemical reaction should depend solely on the experimental data and therefore the process of adsorption which is considered to be the rate-determining step helped in establishing the general order kinetic model. It states that “the order of sorption process

should follow the same trend as that of a chemical reaction", where the order of the reaction is not being restrained by a given model but experimentally [3, 4]. Non-linear form is as following-

$$q_t = q_e - \frac{q_e}{[k_N (q_e)^{n-1}.t.\ (n-1)+1]^{\frac{1}{1-n}}}$$

Where k_N [min^{-1} $(g\ mg^{-1})^{n-1}$] is the rate constant and n is the order of the reaction.

Further, to comment on the dynamics of the sorption and to obtain the information about the rate-limiting steps in the sorption process, we have modelled the kinetic data using Intra-particle diffusion (IPD) model. The equation is as follows[5]

$$q_t = k_i\sqrt{t} + C$$

k_i = intra particle diffusion rate constant (mg/g $hr^{0.5}$) and C gives resistance in mass transfer due to boundary layer

For isotherm experiments, equilibration time was taken as 12h and contaminants concentration in solution was varied in the range of 10-80 mg/L of each metal specie. Obtained experimental data was fitted with the Sip's isotherm model which is a combination of both the famous Langmuir and Freundlich isotherm models. It is helpful in interpretation of sorption on heterogeneous surfaces. Non-linear equation for Sip's adsorption isotherm is-

$$q = q_{max}\frac{K[C_e]^n}{1 + K[C_e]^n}$$

C_e (mg/L) = equilibrium concentration in elute,

q_e = sorption capacity at equilibrium (mg/g),

K = Sips isotherm constant

n = Sips isotherm exponent

It is suitable in predicting sorption for the adsorbents with heterogeneous surfaces [6].

All other parameters were kept same as above. After interaction, reaction mixtures were filtered using 0.22-µm nylon syringe filter and the solutions were acidified and analyzed for remaining metal ions concentration using ICP-OES.

Continuous separation of the contaminants is essential and of crucial importance to ascertain the environmental applications and therefore column experiments were performed. A cylindrical column (11.5 x 0.65 cm) was filled sequentially with sand (1.5 g), sand- SA-Fe^0 composite mixture (900 mg+ 100mg), and sand (1.5 g). The column was packed tightly by adding a piece of sponge at both the ends of the column. The packed column was first saturated with 0.01M $NaNO_3$ solution and then passed with 0.01M $NaNO_3$ solution containing 10 mg/L of each of the metal specie. Elutes were collected in 15 mL vials and analyzed using ICP-OES for released metals concentrations. The flow rate was kept at 0.25 mL/min. Pore volume of the column was 1.2 mL and a total of 300 pore volumes (360 mL) were supplied in the column. Bare sand column was served as frame of reference or blank to compare and comment on the efficiency of the composite. Obtained experimental data were used to plot the breakthrough curves for all the metals and also fitted using the famous Thomas column transport model [7] i.e.

$$\frac{C}{C_0} = \frac{1}{1 + exp(\frac{k_{TH} q_0 m}{v} - k_{TH} C_0 t)}$$

Where:

k_{TH}= Thomas rate constant (mL/min·mg),

q_0= adsorption capacity of the HAP -Fe^0-Ct,

v = flow rate (mL/min),

m = adsorbent weight (g), and

t = breakthrough time (min).

Thomas model doesn't include axial dispersion and assumes Langmuir kinetics process of adsorption-desorption in which 2nd order reversible kinetics is followed by the rate driving force [7].

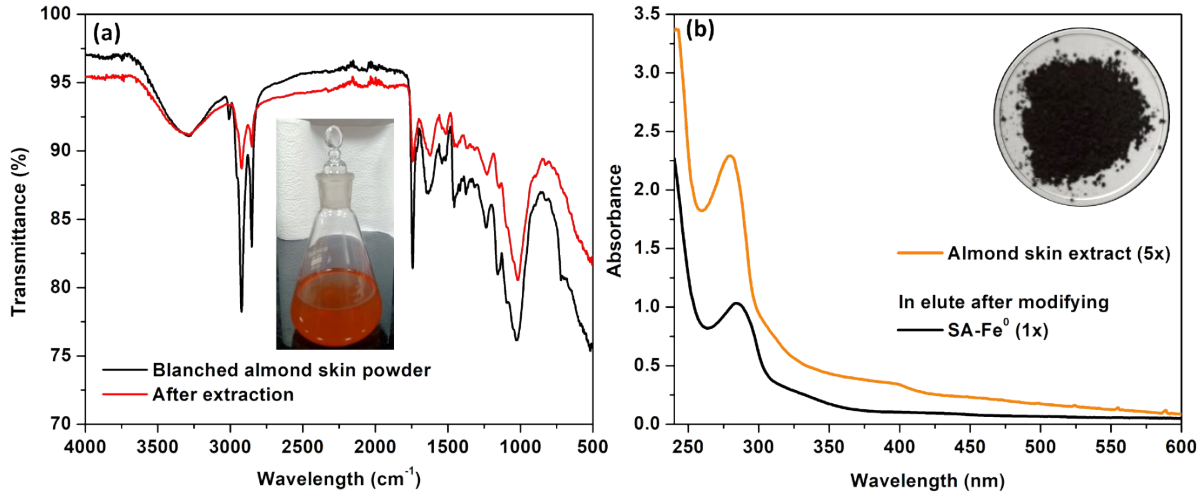

Fig. S1 (a) FTIR spectra of blanched almond skin powder and (b) UV-Vis spectra of antioxidant extract before and after the extraction and interaction with composite, respectively

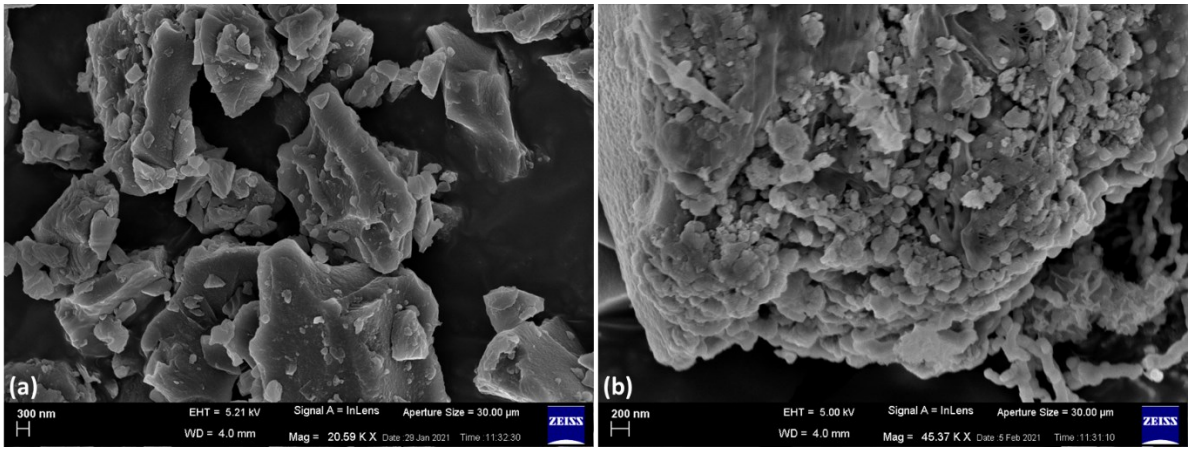

Fig. S2 SEM images of (a) almond shell biochar and (b) SA-Fe^0 composite

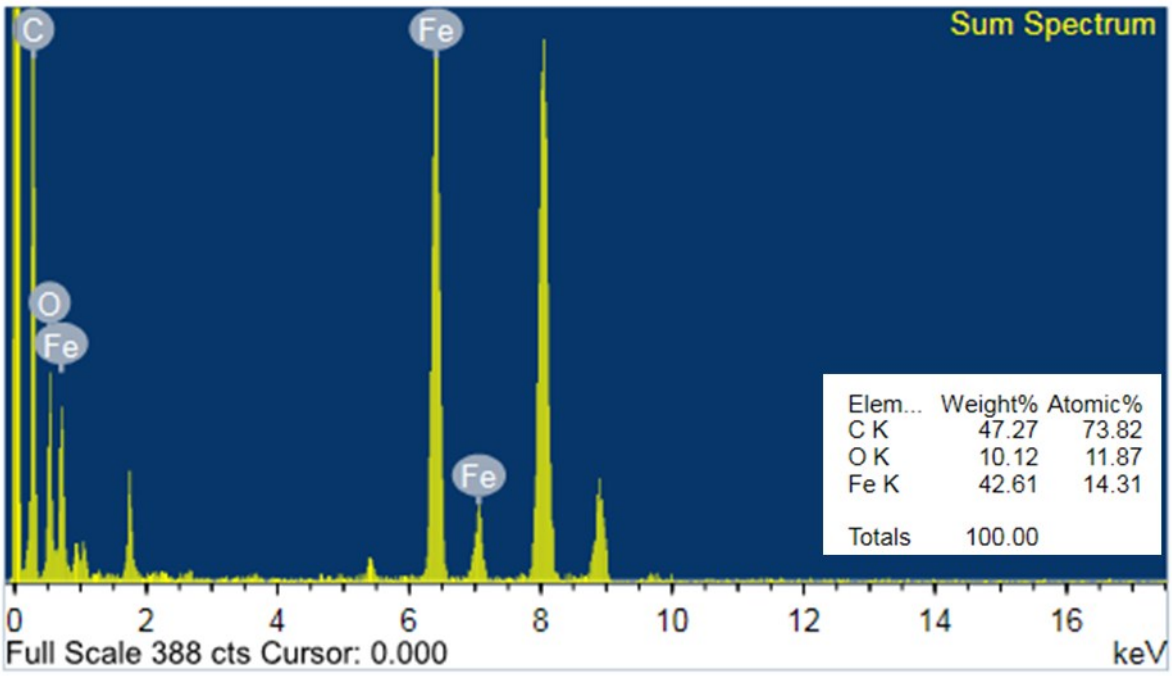

Fig. S3 EDS spectra and composition obtained for SA-Fe^0 composite

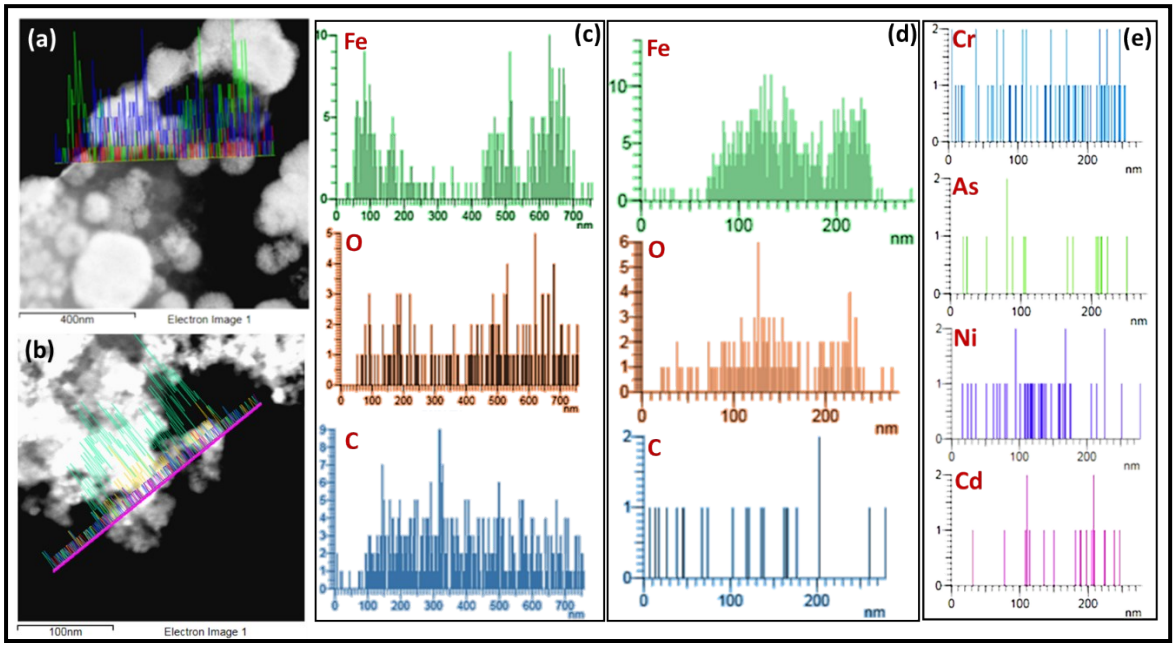

Fig. S4 TEM line scans and elemental distribution along the Fe^0 particles in SA-Fe^0 before (a, c) and after the sorption of metals (b, d, e)

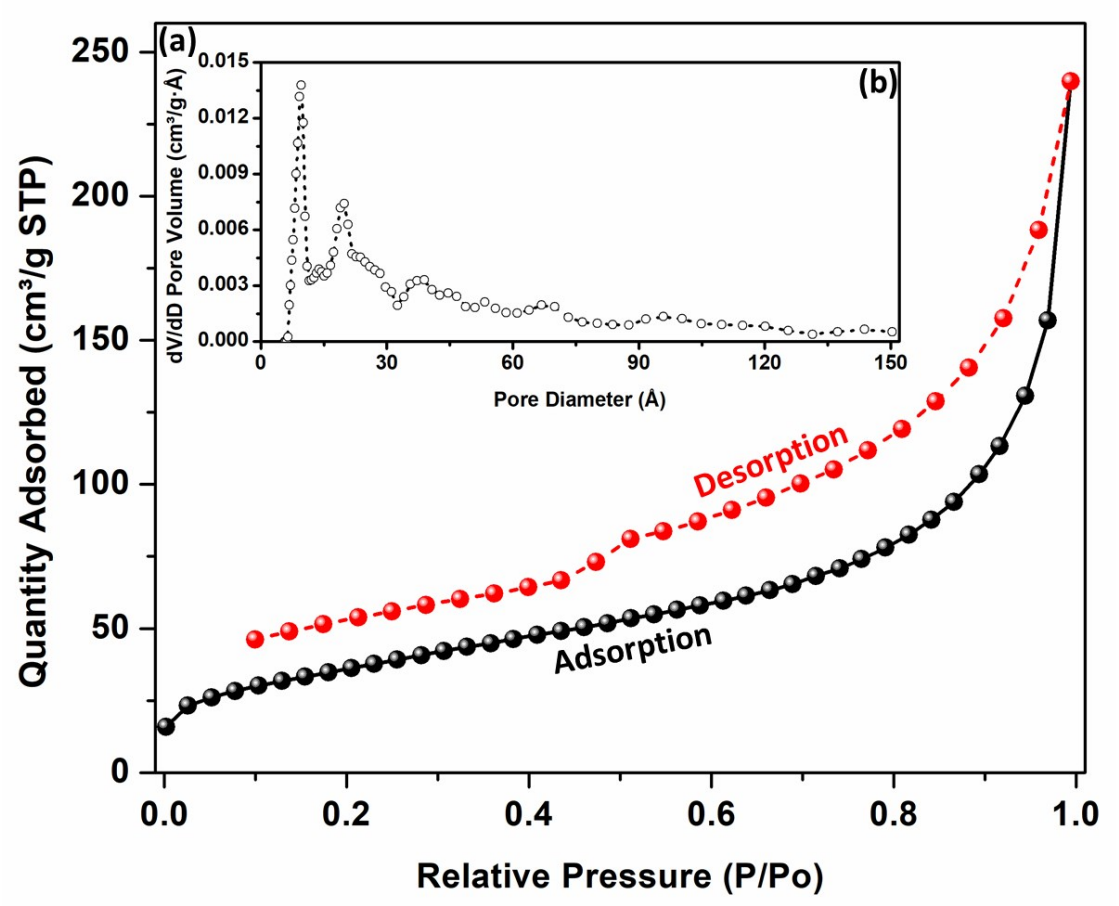

Fig. S5 (a) BET-N_2 sorption- desorption isotherm and (b) pore size distribution obtained for SA-Fe^0

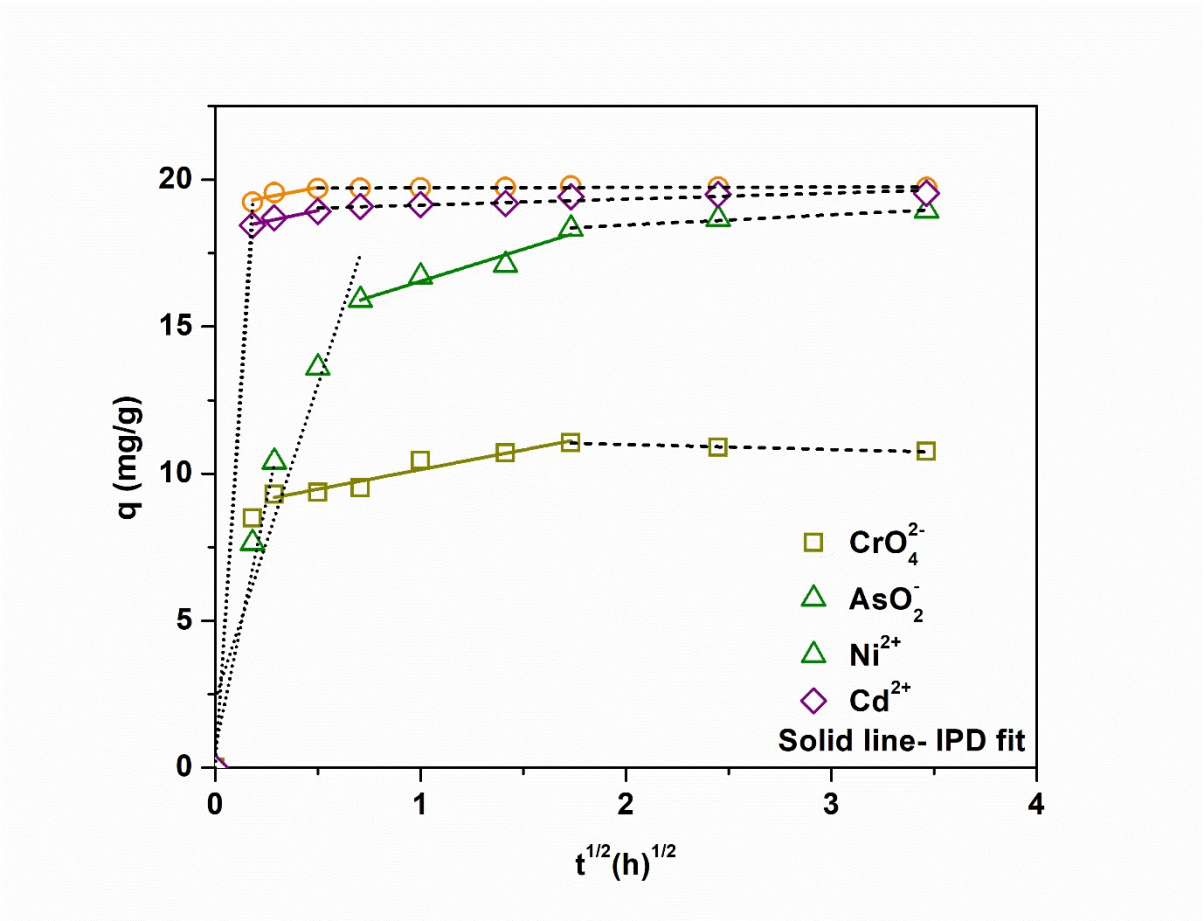

Fig. S6 Intra-particle diffusion modelling of the kinetics data obtained for multi-metallic solutions removal with SA-Fe^0 composite

Section S2: FTIR analysis

Table S1- FTIR peaks and corresponding functionalities [1, 8].

Wavenumbers (cm^{-1})	**Characteristic vibrations (Functionality)**
Almond skin	
3287	-OH stretching due to water or alcohol
3010	stretching vibration of CH *cis*-olefinic groups
2915	CH_3 asymmetric and symmetric stretching
2845	CH_2 asymmetric and symmetric stretching
1740	-COOH
1350-1520	aromatic skeleton vibrations
1238- 1061	presence of lignin and hemicellulose
Biochar	
1694	C=O/ N-H stretching
1585	C=C cyclic alkene stretching
1437	C-H_2 stretching and O-H bending due to alcohol
1378	O=C-O stretching
873	C-H bending (aromatic C-H out-of-plane deformation)
SA-Fe^0	
1630	O-H stretching of H_2O and FeOOH
690	symmetric Fe-O stretching
590	Fe-O stretching modes of tetrahedral and octahedral sites
470	Fe-O stretching due to Hematite

Table S2- model parameters obtained for various models fitted for batch and column sorption experimental data

Models	Parameters	CrO_4^{2-}	AsO_2^-	Ni^{2+}	Cd^{2+}
General Order kinetic model	K_n (min^{-1})	5.38E-02	6.44E-02	1.55E-02	1.94E-02
	q (mg/g)	11.77	20.72	20.48	20.48
	'n'	5.03	13.39	3.44	8.53
	R^2	0.99	1	0.99	1
	RMSE	0.258	0.073	0.27	0.044
	Chi-square	0.067	0.003	0.050	0.001
Intra-particle diffusion (IPD) model	K_i (min^{-1})	1.33	1.34	2.18	1.45
	C	8.8	19.07	14.37	18.22
	R^2	0.92	0.68	0.91	0.91
Sip isotherm model	q_{max} (mg/g)	125.97	300.28	44.54	224.2
	K	0.06	0.37	0.16	0.04
	'n'	0.69	0.5	0.54	0.78
	R^2	0.92	0.85	0.76	0.94
	RMSE	5.094	10.728	5.646	6.316
	Chi-square	4.548	17.648	8.240	20.248
Thomas column transport model	q_0 (mg/g)	1.10E-03	1.10E-03	1.37E-03	1.29E-03
	k_{TH} (L/mg.min)	27.98	27.66	21.55	25.78
	R^2	0.98	0.99	1	0.99
	RMSE	0.034	0.024	0.023	0.03
	Chi-square	0.221	0.159	0.124	0.134

Table S3 Summary of reported adsorbents and their contaminants sorption capacities

Adsorbents	Contaminants				Reference
Capacity (mg/g)	**Ni^{2+}**	**CrO_4^{2-}**	**AsO_2^-**	**Cd^{2+}**	
SA-Fe^0	44.5	125.2	300.2	224.2	**This study**
Biochar-nZVI	47.85	23.09	-	39.53	[9]
Fly ash- Zeolite-nZVI	48.31				[10]
Resin-nZVI			121		[11]
Cellulose@nZVI			92.95		[12]
nZVI/Ze-TiO_2			10.3		[13]
Bentonite supported nZVI	50.25	9			[14, 15]
Pumice-nZVI		306.6 mg/g Fe			[16]
Reduced graphite oxide- nZVI			35.83		[17]
Bentonite-nZVI	16.5			14.25	[15]
CMC-nZVI		87.71			[18]
Activated alumina		25.57			[19]
Nano- alumina	30.82	-			[20]
(nZVI)-Fe_3O_4 nanocomposites		20.41			[21]
Modified activated carbon	78.12	-			[22]
Au-nZVI				40- 188	[23]
Activated carbon (AC)		9.89			[24]

References

1. B. W. Bolling, *Compr Rev Food Sci F*, 2017, **16**, 346-368.
2. N. Khandelwal, M. P. Behera, J. K. Rajak and G. K. Darbha, *Clean Technol Envir*, 2020, **22**, 1015-1024.
3. A. G. N. Wamba, E. C. Lima, S. K. Ndi, P. S. Thue, J. G. Kayem, F. S. Rodembusch, G. S. dos Reis and W. S. de Alencar, *Environ Sci Pollut R*, 2017, **24**, 21807-21820.
4. Y. Liu and L. Shen, *Biochem Eng J*, 2008, **38**, 390-394.
5. J.-P. Simonin and J. Bouté, *Revista Mexicana De Ingenieria Quimica*, 2016, **15**, 161-173.
6. A. Nimibofa, A. Ebelegi and W. Donbebe, *Hindawi Journal of Chemistry*, 2017, **Volume 2017**, 11 pages.
7. Z. Z. Chowdhury, S. M. Zain, A. K. Rashid, R. F. Rafique and K. Khalid, *J Chem-Ny*, 2013, **2013**, 959761.
8. A. Liu and W.-x. Zhang, *Analyst*, 2014, **139**, 4512-4518.
9. S. S. Zhu, S. H. Ho, X. C. Huang, D. W. Wang, F. Yang, L. Wang, C. Y. Wang, X. D. Cao and F. Ma, *Acs Sustain Chem Eng*, 2017, **5**, 9673-9682.
10. G. K. R. Angaru, Y. L. Choi, L. P. Lingamdinne, J. S. Choi, D. S. Kim, J. R. Koduru, J. K. Yang and Y. Y. Chang, *Chemosphere*, 2021, **267**.
11. Q. Du, S. J. Zhang, B. C. Pan, L. Lv, W. M. Zhang and Q. X. Zhang, *Water Res*, 2013, **47**, 6064-6074.
12. S. M. Zhou, D. Wang, H. Y. Sun, J. T. Chen, S. H. Wu and P. Na, *Water Air Soil Poll*, 2014, **225**.
13. S. Madan, R. C. Shaw, S. Tiwari and S. K. Tiwari, *Colloid Surface A*, 2020, **607**.
14. L. N. Shi, X. Zhang and Z. L. Chen, *Water Res*, 2011, **45**, 886-892.
15. N. A. Zarime, W. Z. W. Yaacob and H. Jamil, *AIP Conference Proceedings*, 2018, **1940**, 020029.
16. T. Y. Liu, Z. L. Wang, X. X. Yan and B. Zhang, *Chem Eng J*, 2014, **245**, 34-40.
17. C. Wang, H. J. Luo, Z. L. Zhang, Y. Wu, J. Zhang and S. W. Chen, *J Hazard Mater*, 2014, **268**, 124-131.
18. N. Kumar, A. Kardam, D. S. Rajawat, V. K. Jain and Suman, *Mater Res Express*, 2019, **6**.
19. A. K. Bhattacharya, T. K. Naiya, S. N. Mandal and S. K. Das, *Chem Eng J*, 2008, **137**, 529-541.
20. V. Srivastava, C. H. Weng, V. K. Singh and Y. C. Sharma, *Journal of Chemical & Engineering Data*, 2011, **56**, 1414-1422.
21. X. S. Lv, Y. J. Hu, J. Tang, T. T. Sheng, G. M. Jiang and X. H. Xu, *Chem Eng J*, 2013, **218**, 55-64.
22. M. O. Abd El-Magied, A. M. A. Hassan, H. M. H. Gad, T. F. Mohammaden and M. A. M. Youssef, *Journal of Dispersion Science and Technology*, 2018, **39**, 862-873.
23. Y. Su, A. S. Adeleye, Y. Huang, X. Sun, C. Dai, X. Zhou, Y. Zhang and A. A. Keller, *Water Res*, 2014, **63**, 102-111.
24. S. Mortazavian, H. An, D. Chun and J. Moon, *Chem Eng J*, 2018, **353**, 781-795.